On the design of measuring circuit for OCVD method

V. Papež and J. Hájek,
Department of Electrotechnology
Faculty of Electrical Engineering, CTU in Prague
166 27 Prague 6, Czech Republic

Abstract

The article deals with the matter that is often omitted by authors – design of measuring circuit. The most of publications describe theoretical background of the OCVD method or they interpret results obtained on modern SiC or 4H-SiC structures. But correct and relevant results are conditioned by corresponding measuring circuit. Even if the OCVD method is based "just" on recording of voltage response, measuring circuit must fulfill a lot of requirements from high-frequency techniques. Following article tries to explain these techniques.

Keywords: OCVD, lifetime, transient effects, damping, inductance-less sensing.

PRINCIPLES OF OCVD METHOD

In homogenous PN junction, where only one generation-recombination mechanism exists, can appear specific voltage response. This voltage response is detectable immediately after the forward current bias through the PN junction disappears [1]. Voltage response exhibits nearly linear decline and this slope can be used for the determination of so-called charge carrier lifetime [2]. With some simplification the voltage decline on the P-NN+ diode structure is given by the following expression:

$$V(t) = V_P(t) + V_N(t) - \int_0^w E(x;t)dx\,, \qquad (1)$$

where V_P is the decrease of voltage at PN junction, V_N is the decrease of voltage at NN^+ junction and E is the local electric filed in the basis according equation:

$$E(x,t) = -\frac{J(x;t)}{e(\mu_n + \mu_p)\Delta n(x;t)} - \frac{kT(\mu_n - \mu_p)}{e(\mu_n + \mu_p)\Delta n(x;t)}\frac{d\Delta n(x;t)}{dx}. \qquad (2)$$

Voltages on both junctions are described by Boltzmann's expressions:

$$\frac{p_N(0,t)}{N_A^+} = \exp\left\{\frac{-e[\varphi_P - V_P(t)]}{kT}\right\}, \qquad (3)$$

$$\frac{n_N(w,t)}{N_D^+} = \exp\left\{\frac{-e[\varphi_N - V_N(t)]}{kT}\right\}. \qquad (4)$$

Trash-hold voltages on both junctions P-N and NN^+ are given by the equations:

$$\varphi_P = \left(\frac{kT}{e}\right)\ln\left(\frac{N_A^+ N_D}{n_i^2}\right), \qquad (5)$$

$$\varphi_N = \left(\frac{kT}{e}\right)\ln\left(\frac{N_N^+ N_D}{n_i^2}\right). \qquad (6)$$

When we considered constant lifetime, the concentration of free charge carriers is reduced in time due to the recombination process according following expressions:

$$p_N(0;t) = p_N(0;0)\exp\left(-\frac{t}{\tau}\right), \qquad (7)$$

$$n_N(w;t) = n_N(w;0)\exp\left(-\frac{t}{\tau}\right). \qquad (8)$$

If we can neglect the internal electric field in the basis, we can obtain (based on Eq. 1, 3 and 4) the final equation for lifetime of free charge carriers:

$$\tau = -\alpha\frac{kT}{e}\left(\frac{dV}{dt}\right)^{-1}, \qquad (9)$$

where α is some constant near to 1 in the case of low injection conditions and near to the value 2 in the case of high injection conditions [3].

DESIGN'S ASPECTS OF MEASURING CIRCUIT

The OCVD method is on the most used method for the lifetime determination for most diode structures. The basis of the method is in the idealized theoretical analysis of the charge distribution in the PN junction region and related transient effects in semiconductor bulk. When the influence of measuring circuit on the transport and transient effects in semiconductor is omitted, measured values will deeply differ from the correct (real) values. Ideal waveform of forward voltage $V_F(t)$ on PN junction is marked on the Fig. 1a. The sample is supplied from the constant current source or from the voltage source with serial resistance through the switch S (near to ideal). The PN junction is biased by forward current and constant voltage drop can be observed. After the disconnection of forward current, the forward voltage drop immediately fall down and consequently we can observe linear voltage decline with the constant rate $\mathrm{d}V_F/\mathrm{d}t$.

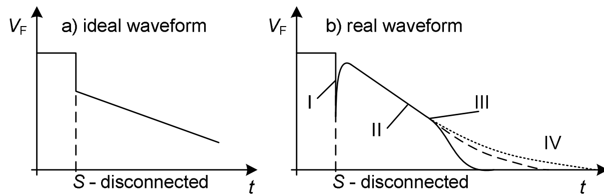

Fig. 1 Ideal and real voltage waveforms at PN junction.

Observed waveforms in real circuits are usually totally different as shown on Fig. 1b. The voltage waveform is (in the region I) distorted by the transient effect coming from the switch S disconnection. The root cause is the fact that the real voltage source is not ideal and has to be substituted at least by the RLC resonant circuit.

In the circuit there is a transient effect of the 2nd order which can be a quasi-periodic process. As the consequence we can observe short-term reversing of forward current in the PN junction and sharp decline of the voltage. Such situation leads to the fast reduction of free charge carriers in the PN junction. But this is a serious violation of theoretical conditions [4].

If the PN junction is biased by the current with dominant diffusion current, the voltage waveform differs at least from the ideal in the region II. The searched lifetime of carriers can be determined by the falling rate of $\mathrm{d}V_F/\mathrm{d}t$. The V_F waveform exhibits more slopes in this region if there are multiple generation-recombination processes in the PN junction with longer lifetimes. The derivation process applied during the evaluation of measurement will cause an increase of the noise and distortion; i.e. this effect must be minimized.

In the region III there is significantly visible deviation between real and ideal (linear) voltage decline. One of the possible explanations of this follows: The recombination current of charge carriers is not the dominant part of current flowing through the PN junction. The transient effect starts to be a discharging process of barrier capacity by the diffusion current or external admittance [5], [6].

In the region IV there is a voltage decline with exponential shape when the time constant is given by the total capacity and total conductivity of measured diode. If we considered a connection of external positive susceptance and small conductance, then we can obtain a time constant much bigger than in the region II. It is highlighted by dotted line on Fig. 1b. On the other hand, by connecting huge external conductivity or by the generation of photovoltaic current the time constant is significantly reduced as it is shown by solid line on the Fig. 1b.

When we think about real values of capacities and conductances that could be connected to the measured sample, we can say that specifications on power discrete devices are not strict too much. Externally connected conductance lower than cca 1 μS/cm^2 and capacity lower than 30–50 pF/cm^2 of the PN junction can not significantly affect the measurement and they can cause only the measurement error of percent units. Voltage waveform can be sensed directly by the DSO with sample rate higher than cca 1 GSa/s and with a high-impedance input or with the usage of passive probe [8].

The other important part of the OCVD tester determining its features is the current source. It provides impulses of forward current for the measured sample (DUT) which do not differ from the rectangular shape. Moreover, between pulses the source must have high impedance from the sample (DUT) point of view. The basic parameters of the source (often not specified) are:

- the amplitude of forward current and the $\mathrm{d}i/\mathrm{d}t$ falling slope at the end of pulse (turn-off time),
- damping of the current overshoot at the falling slope,
- duration of the pulse and repeating frequency,
- the generated noise-level and the impedance of the disconnected source.

The oldest and the simplest design of the source is the generator with the diode switch according the principal diagram on the Fig. 2a [1], [7]. The amplitude and the shape of pulses corresponds with the used impulse generator and they reach from 0.1 A to the maximum 1 A with the turn-off time about 10 ns. When the switch is disconnected, its conductance is typically lower than 1 μS and the capacity is in the range units or tens of pF. Such design is useful for the measurement of samples with the area of tenth up to tens of mm^2. For bigger samples it does not supply enough current.

The generator with the mercury (Hg) relay shown on the Fig. 2b presents idealized design [1], [9]. The generator can supply current of several amperes and it provides the fastest disconnection from all mechanical equipments in the order of tens of ns. In the OFF-state its capacity is only several pF and its conductance is several nS [11]. The main disadvantage of Hg-relay is to long time-delay between the coil current and the switching process. This delay significantly limits the maximum frequency of pulses up to several tens of Hz.

In addition, the time delay is random, i.e. the delays between individual processes are variable.

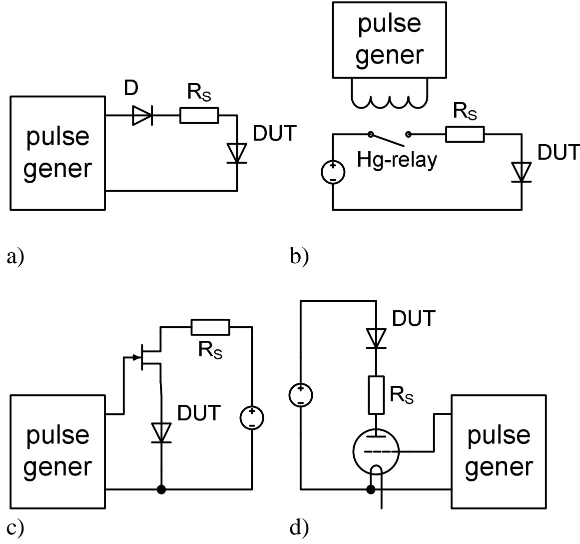

Fig. 2 Possible designs of generator for OCVD circuit.

This effect makes totally impossible synchronous evaluation of consecutive measurement; this technique is usually used by digital signal processing. Described Hg-relays are suitable – thanks to low admittance of disconnected contacts – especially for the measurement on smallest samples. Applying currents about 1 A declines the durability and reliability of contacts.

The generator with semiconductor switch [7] on the Fig. 2c enables very good matching between the circuit and measurement's requirements [5], [11]. With using of small-power switching transistors we can generate pulses with the amplitude of several amperes and turn-off time several ns. With the use of power MOSFETs the pulses with amplitude of 100 A and turn-off time of several tens of ns can be generate. The conductance of the disconnected switch is typically lower than 1 μS and the capacity is in the order units or tens of pF. The disadvantage of this switch is the possibility of current-overshoot generation during the turn-off process and the need to suppress this overshoot. The design of the switch can be adapted for the measurement of samples with the area of 10^{-2} cm^2 up to 10^2 cm^2 or for the measurement with the highest current.

The generator with vacuum tube shown on the Fig. 2d enables to generate pulses with the amplitude several tens of amperes and with the turn-off time tens of ns [7]. When it is disconnected it has negligible conductivity and the capacity units or tens of pF. The serial resistance 10 Ω effectively suppresses overshoots and oscillations during the turning-off process. The main disadvantage of vacuum tube is the need of high-voltage source and tube heating.

REALIZED CIRCUIT

The real switch of forward current can be simply analyzed by means of equivalent RLC circuit shown on the Fig. 3. V_{IN} is the supplying DC voltage source, C is the capacity of disconnected switch S, R is the resistor for current adjustment, L is the parasitic inductance of interconnection, C_D and R_D are components of the admittance of opened DUT. Due to the following relations ($R_D << R$ and $C_D >> C$) the diode in ON-state can be consider as a short circuit and the transient aperiodic effect during turning-off can be described as follows (10) and (11):

$$\frac{d^2 i(t)}{dt^2} + \frac{R}{L}\frac{di(t)}{dt} + \frac{i(t)}{LC} = 0\,, \tag{10}$$

$$\sqrt{\frac{L}{C}} < \frac{R}{2}\,. \tag{11}$$

The estimation $R \sim 1\ \Omega$, $C \sim 100$ pF can be used for currents in the circuit higher than 10 A. To keep the condition for aperiodicity (11) it is necessary to ensure $L < 0.025$ nH; that is practically impossible. The solution by increasing the resistivity R or the capacity C is not possible; the supplying voltage will increase too much, and voltage response will distort [9].

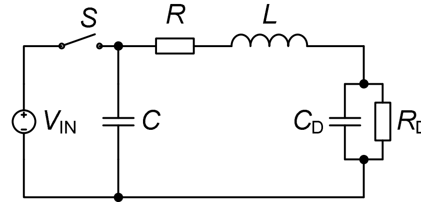

Fig. 3 Real switch presented as an RLC circuit.

The resonance can be damped by R_D that is connected to the inductance L in parallel [6]. The oscillations are minimized when the resistivity is closed to the reactance of the L at the resonance frequency of the circuit. For the real values from the circuit on Fig. 3 the reactance of L is about 3.16 Ω ($R_S = 0.4\ \Omega$; $C_P = 400$ pF; $L_S = 4$ nH; self-resonance frequency is 125 MHz). The voltage and current waveforms were simulated in LTspice according simplified circuit from the Fig. 4. Different parasitic inductances and different damping were reflected.

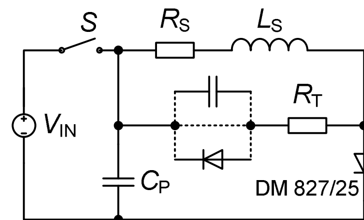

Fig. 4 Substitution circuit of the switch in LTspice simulation.

Waveforms on the Fig. 5 are shifted in time intentionally for better understanding. The first waveform from the left shows the real circuit with optimal damping. Waveforms are overshoots-free. The 2nd waveform shows the circuit with the same real inductance and low damping. There is no visible periodic oscillation. The 3rd waveform shows the circuit with big inductance and optimal damping. Both waveforms (voltage, current) show aperiodic overshoot. The last fourth waveform shows the circuit with big inductance and minimal damping. Both (voltage and current) waveforms show periodic damped oscillations. It is useful to connect the damping resistor with the main circuit through separating capacity or diode. Then the resistor is loaded by current only during overshoots. This solution will reduce power losses and does not affect forward current through the R_S except rising and falling slopes of the pulse.

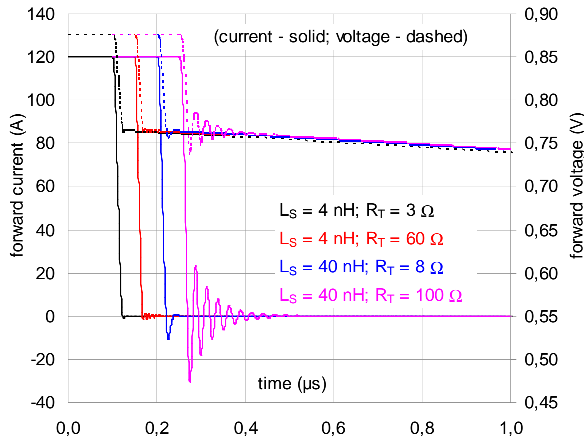

Fig. 5 LTspice simulation of the circuit on the Fig. 4.

Realized circuit with depicted real and parasitic parameters is shown on the Fig. 6. Two parallel connected SiC MOSFETs type C3M0075120 are used as a switch S. Both MOSFETs are controlled by trigger signal from galvanic-isolated generator. The maximum forward current I_F through DUT is limited by series resistance R_S (0.36 Ω). Resistor is made by three parallel connected power foil-resistors BDS100 produced by TE-Connectivity with the nominal value of 1 Ω and inductance 6 nH [12]. Thus, the maximum forward current I_F is set to 140 A with supplying voltage 52 V. The voltage source V_{SS} is equipped by blocking capacity C that consist from four electrolytic capacitors 10 mF/50 V type B41231 connected in parallel; 16 electrolytic capacitors 1 mF/50 V type WCAP-ASLI and four capacitors 10 µF/63 V type F161. Individual capacitors are interconnected “as a matrix” by means of parallel-plate transmission line with the dimension 100×120 mm and characteristic impedance about 3 Ω. The total capacity is cca 60 mF; ESR is cca 1 mΩ and self-inductances are lower than 1 nH. The layout of capacitor battery is on the Fig. 8. Elements L_{S1} and L_{S2} represent the inductances between tested diode and the measuring circuit. Both elements are realized as a “triplate stripline” with the characteristic impedance cca 2 Ω and with the length 100 mm. This connection shows the total inductance cca 2 nH plus the inductance of R_S. Two damping resistor R_{T1}, R_{T2} are 2.2Ω resp. 1.5Ω and are made by parallel combination of SMD thick-film resistors 22 Ω/1 W type CRCW1218.

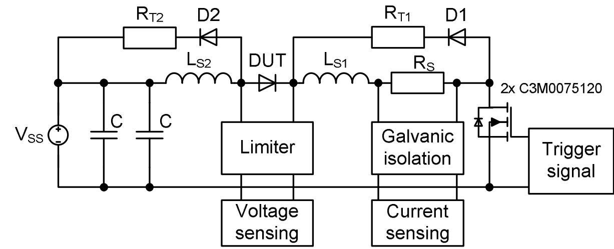

Fig. 6 Circuit design of the real OCVD tester.

Waveforms on PN junction $V_{DUT}(t)$ and $I_{DUT}(t)$ were observed by the oscilloscope KEYSIGHT DSOX2022A that provides bandwidth 200 MHz, sampling rate 2 GSa/s and 8bit resolution (see Fig. 7). Waveforms were recorded with the averaging function (64×). It makes better the S/N ratio by approx. of 20 dB in comparison with individual recording.

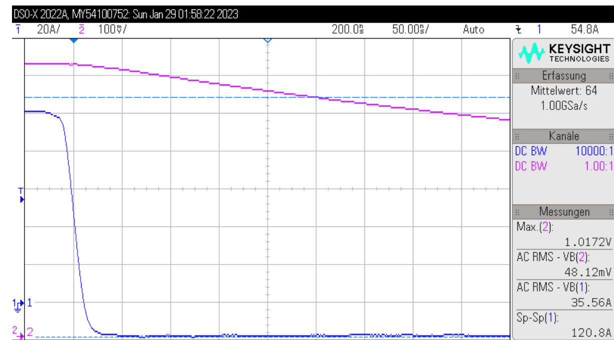

Fig. 7 Waveforms of $V_{DUT}(t)$ and $I_{DUT}(t)$ recorded by DSO.

The limiter protects the oscilloscope’s input against overvoltage coming from the DUT’s outlets when the circuit disconnect. The limitation voltage level is ±5 V; the time-constant is lower than 30 ns. Current waveform is evaluated as a voltage drop on the resistor R_S. To the R_S is as a shunt connected another resistor and its current (few hundred of mA) is sensed by the current probe Agilent N2774A. In this way the galvanic separation between the oscilloscope and current probe is ensured. The rate of falling slope dI_{DUT}/dt is cca 4 A/ns.

Fig. 8 Layout of the inductance-less battery of capacitors.

On the Fig. 9 there are really measured and simulated waveforms of $V_{DUT}(t)$ and $I_{DUT}(t)$ obtained during the measurement on soft commutated diode DM 827/25 and in the circuit with optimal damping. There are no significant differences between measured and simulated curves. The measuring circuit ensures forward currents in the range from 1 A up to 140 A and with the pulse length 100 µs up to 1 ms and repeating frequency 10 Hz. Proper combination of the pulse length and repeating frequency is assumed to keep the total power bellow 100 W.

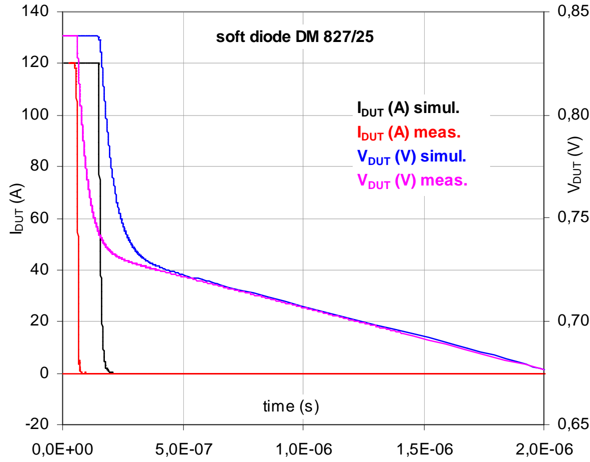

Fig. 9 The comparison of simulated and measured waveforms on soft commutated diode DM 827/25 (irradiated device).

MEASUREMENTS AND INTERPRETATIONS

The circuit shown on the Fig. 6a and described in previous chapter has been realized in the 2022 and beginning the 2023 the verification measurements started. The main goal of verification was to identify the lifetimes at high-injection conditions and compare them with expected values. The next task was to determine the influence of forward current I_{DUT} on the measured lifetime. The current was chosen in the set 1-10-100 A. Power diodes with totally different design and parameters were chosen as the samples to obtain results in a wide range of lifetimes. Three main types are described in the text bellow.

The samples' current I_{DUT} was controlled by supplying voltage V_{SS}. The waveforms of forward voltage drop V_{DUT} were sensed by the oscilloscope DSOX2022A as it is described in previous text. Waveforms were used for numeric calculation of lifetimes according (9). The importance of proper and noise-free sensing of voltage signals is obvious. Measured levels are hundred mV high and declines in time. The typical 8bit resolution of commonly used AD converters is often not enough for exact calculation. The adjacent samples differ just by the LSB value or less even they are the same. Then the calculation according (9) failed. This is the root-cause of quantization noise shown on the Fig. 13 and Fig. 15.

Measurement on 2' avalanche diode

Large avalanche diodes are mostly designed as P-i-N diodes with thick Si-wafer (750 µm) and with the initial bulk resistivity in the range 150-250 Ωcm. Lifetimes are long and not controlled. Values in the order of hundred µs are expected. This is given only by the cleanness of initial bulk and diffusion process.

In the area of linear decline of V_{DUT} (cca 1 ms on the Fig. 10) we can obtain from the Fig. 11 relatively constant and I_{DUT} independent two lifetimes (τ_{n0} ~ 300 µs; τ_{p0} ~ 120 µs). The quantization is given by sampling and following digital processing.

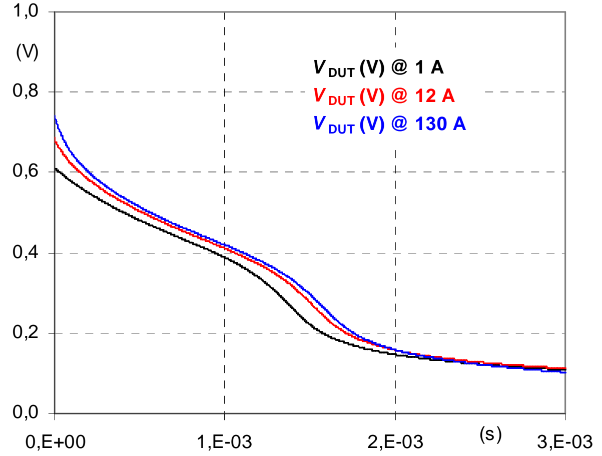

Fig. 10 Decline of forward voltage V_{DUT} on the 2' avalanche diode for three different forward currents I_{DUT} (not shown).

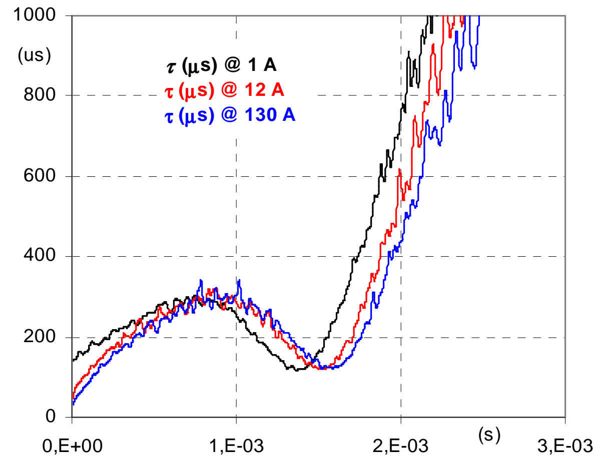

Fig. 11 Numerically counted lifetimes for the avalanche diode biased by the forward current density 0.05; 0.5; 5 A/cm^2.

Measurement on 40mm soft diode

Fast diodes with soft commutation are mostly designed as a junction with compressed electric field with the wafer thickness 400-500 µm and initial resistivity 100-150 Ωcm. The lifetime is reduced to units or tens of µs by electron beam irradiation or by accelerated protons or by the diffusion of heavy metals (like Au, Pt, etc).

In the area of linear decline of V_{DUT} (cca 50 µs on the Fig. 12) we can obtain from the Fig. 13 relatively constant and I_{DUT} independent lifetimes (τ_{n0} ~ 15 µs, τ_{p0} ~ 16 µs). The quantization is given by sampling and following digital processing (especially at the time above 100 µs).

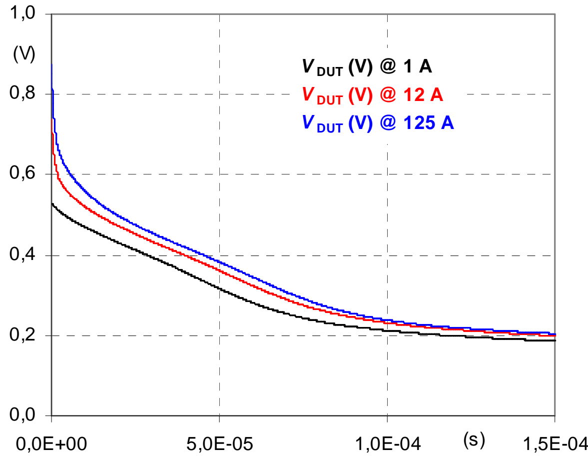

Fig. 12 Decline of forward voltage V_{DUT} on the fast (soft) diode for three different forward currents I_{DUT} (not shown).

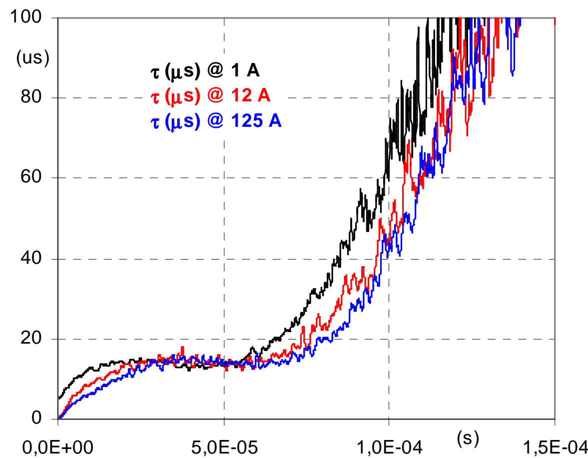

Fig. 13 Numerically counted lifetimes for the soft diode biased by the forward current density 0.1; 1.0; 10 A/cm^2.

Measurement on 2.5' welding diode

Welding diodes are very specific power rectifier diodes. Their design is optimized for extremely high forward current density (I_{FAV} ~ 10 kA). This is paid by very low reverse breakdown voltage; V_R is typically 400 V. Diodes are made from Si-wafer with the thickness about 200 µm and with very low initial bulk resistivity (10 Ωcm). The carrier's lifetime is not controlled and is generally very low. The typical value is units of µs.
In the area of linear decline of V_{DUT} (cca 50 µs on the Fig. 14) we can obtain from the Fig. 15 two values of lifetime (τ_{n0} ~ 14 µs, resp. τ_{p0} ~ 9 µs). They don't depend on the I_{DUT} current. The quantization is given by sampling and following digital processing.

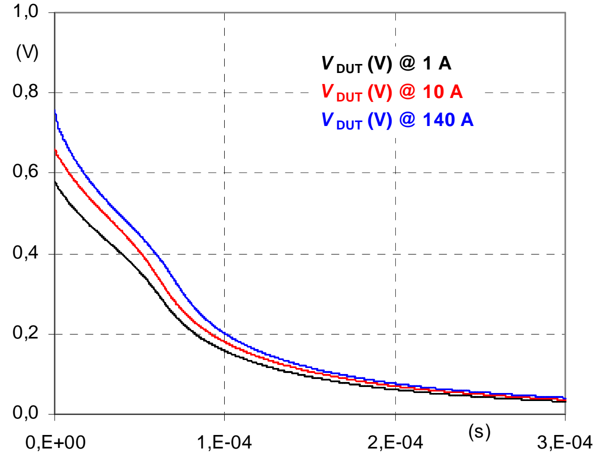

Fig. 14 Decline of forward voltage V_{DUT} on 2.5' welding diode for three different forward currents I_{DUT} (not shown).

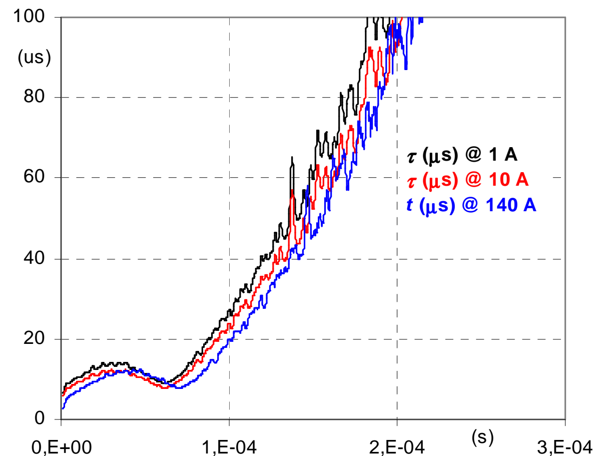

Fig. 15 Numerically counted lifetimes for the welding diode biased by the forward current density 0.05; 0.5; 5 A/cm^2.

SUMMARY

This article describes design's issues and main rules of the testing circuit for the OCVD method. The attention is paid especially to proper damping and suppressing of all undesired oscillation and transient effects that can influence measured waveforms and numerically processed lifetimes. The correctness of described recommendation is documented by the measurements of the set of different samples. They exhibit totally different lifetimes. The measurements were performed with the current density varying from 0.01 A/cm^2 to 10 A/cm^2. Expected lifetimes of electrons (τ_{n0}) and holes (τ_{p0}) at high-level injection were confirmed. Based on the Figs. 11, 13 and 15 we can say that the applied current density does not have any significant influence on the measured carrier's lifetime. Forward current affects only the very beginning of the voltage transient waveform.

ACKNOWLEDGEMENTS

The authors wish to express many thanks to the company Hitachi Energy Czech Republic s.r.o for giving samples of Si-wafers and soft diodes and to the company Tesla V.T. Mikroel for the electron irradiation of these diode samples.

REFERENCES

[1] Lederhandler, S.J., Giacoletto, L.J: Measurement of minority carrier lifetime and surface effects in junction devices, Proceedings of the IRE, **43**, 1955, 477-483.

[2] Benda, V., Černík, M., Papež, V.: OCVD carrier lifetime in P^+NN^+ diode structures with axial carrier lifetime gradient, Microelectronics Journal, **37**, 2006, 217-222.

[3] Siemieniec, R., Südkamp, W., Lutz, J.: Determination of parameters of radiation induced traps in silicon. Solid-State Electronics, **46**, 2002, 891-901, DOI: 10.1016/S0038-1101(01)00321-5.

[4] Benda, V.: Carrier Lifetime Control in Power Semi-conductor Devices, Proceedings of the XIV. International Workshop on the Physics of IEEE, (2007), 755-761, ISBN 978-1-4244-1727-8.

[5] Lemaire, A., Perona, A., Caussanel, M., Duval, H.: Open Circuit Voltage Decay: Moving to a Flexible Method of Characterization, IET Circuits, Devices & Systems, **14**, 2020, 947-955, DOI: 10.1049/iet-cds.2020.0123.

[6] Papež, V., Hájek, J., Horák, M., Künzel, K.: Analysis of the measuring circuit for the OCVD method, ISPS'18 Proceedings. 14th International Seminar on Power Semiconductor, (2018), 123-131, ISBN 978-80-01-06469-6.

[7] Ivanov, P.A., Levinshtein, M.E., Irvine, K.G., Kordina, O., Palmour, J.W.: High hole lifetime (3.8 μs) in 4H-SiC diodes with 5.5 kV blocking voltage, Electronics Letters, **35**, 1999, 1382-1383, DOI: 10.1049/el:19990897.

[8] Bellone, S., Licciardo, G.D: An Analog Circuit for Accurate OCVD Measurements, IEEE Transaction on Instrumentation and Measurement, **57**, (2008), 1112-1117, DOI: 10.1109/TIM.2007.915468.

[9] Sozzi, G., Sapienza, S., Nipoti, R., Chiorboli, G.: OCVD Measurement of Ambipolar and Minority Carrier Lifetime in 4H-SiC Devices: Relevance of the Measurement Setup, IEEE Transaction on Electron Devices, **68**, (2021), 3254-3260, DOI: 10.1109/TED.2021.3083211.

[10] Sozzi, G., Puzzanghera, M., Chiorboli, G., Nipoti, R.: OCVD Lifetime Measurements on 4H-SiC Bipolar Planar Diodes: Dependences on Carrier Injection and Diode Area, IEEE Transaction on Electron Devices, **64**, (2017), 2572-2578, DOI: 10.1109/TED.2017.2691280.

[11] Tapajna, M., Pjenčák, J., Vrbický, A., Harmatha, L., Kúdela, P.: Application of open circuit voltage decay to the characterization of epitaxial layer, Advances in Electrical and Electronic Engineering, **3**, (2011),
DOI: 10.15598/aeee.v3i2.432.

[12] Lacouture, S., Schrock, J., Hirsch, E., Bayne, S., O'Brien, H.: Ogunniyi, A.: An open circuit voltage decay system for performing injection dependent lifetime spectroscopy, Review of Scientific Instruments, **88**, 2017, 95-105, DOI: https://doi.org/10.1063/1.5001732.

[13] On-line (2023-07-04), Surface Mount Reed Relays Series Pickering 200: https://pickeringrelay.com/pdfs/200-surface-mount-reed-relays.pdf.

[14] On-line (2023-07-04) Thick Film Power Resistors Type BDS100 Series: https://datasheet.octopart.com/1614783-2-TE-Connectivity---AMP-datasheet-17726072.pdf.

Addresses of the authors

Papež V., CTU in Prague, Technická 2, 166 27 Prague, CZ, papez@fel.cvut.cz
Hájek J., CTU in Prague, Technická 2, 166 27 Prague, CZ, hajekj1@fel.cvut.cz